Encyclopedia of Tribology and Lubrication

Wear

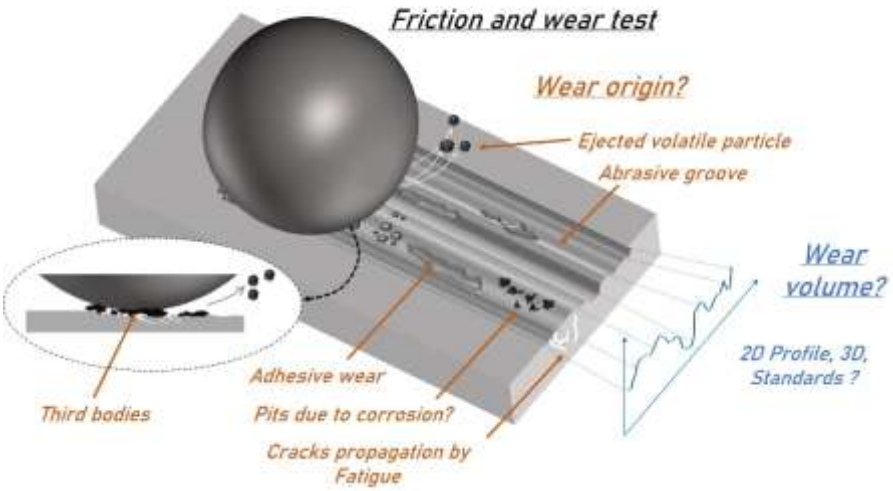
Guillaume COLAS

Université Marie et Louis Pasteur, CNRS, institut FEMTO-ST, F-25000 Besançon, France

Abstract

Wear is responsible for up to 4% of the global energy consumption, hundreds of tons of CO_2 emission every year, and microparticle emissions. Managing wear and increase wear life of tribosystems is a key to reduce its environmental footprint. To manage it, it is essential to understand it. However, wear definition is still debated. The concept of wear and quantification will hence be discussed to hopefully bring the reader enough information and self-questioning on how to address wear in tribocontacts. Throughout this chapter, different types of wear are discussed, as well as some approaches to quantify, understand, and predict it.

Graphical Abstract



Keywords

Wear, friction, tribology, abrasion, adhesive wear, tribocorrosion, fatigue wear, Archard, wear volume calculation, third body

Keypoints

- Wear is a system response
- Wear is a multiphysics phenomenon
- Wear « modes » are usually combined
- Wear modes can change over time
- Wear volume calculations can be subjected to large errors

Table of Content

1 Introduction 2
2 The usual approach to consider wear 2
2.1 Adhesive wear 3
2.2 Abrasive Wear 6
2.2.1 Fatigue wear 7
2.3 Corrosive wear 9
2.4 And now? 11
3 Third body concept in this framework of wear studies 11
4 Understanding the origin of wear 14
5 Quantification of Wear volume? 15
6 Conclusion 17
7 References 18

1 Introduction

Based on Cambridge dictionary, Wear is defined as a noun or as a verb. As a noun it refers to "the amount or type of use an object has had or can be expected to have" or to the "damage caused to something by using it a lot". As a verb, it consists in "becoming weaker, damaged, or thinner because of continuous use" or in "producing something such as a hole or loss of material by continuous use, rubbing, or movement". Tribologically speaking, it often referred to the amount of material removed from two or three bodies, initially in contact, and that have been submitted to continuous rolling and/or sliding. Wear originates from different mechanical and physicochemical processes, making it hard to fully undertake while developing tribosystems, and which also makes it hard to predict. Moreover, "wear is not a material property, it is a system response" [1]. It has been elegantly demonstrated early in the 80s by kohen et al [2]. Relying only on wear volumes is not sufficient and deep understanding of the physical, mechanical, and chemical mechanisms involved in wear is necessary [3–5].

As wear is a system response, it is difficult to predict. This is a reason why wear remains responsible for 3 to 4% of the global energy consumption and to hundreds of tons of CO_2 emission every year [6]. Wear is also the source of microparticle emission contributing to air pollution and health hazard [7–9]. Managing wear and increase wear life of tribosystems is a key issue to reduce the environmental footprint of tribology. To manage it, it is essential to understand it.

Wear is such a broad topic, that it can be the subject of an entire book in itself. Hundreds of wear equations can be drawn, and wear happens at all scales (from macro to nano). Throughout this chapter, different types of wear will be briefly presented, as well as some approaches and models that aimed at quantifying and predicting it. Wear definition is still debated, that is why the concept of wear and quantification will be discussed to hopefully bring the reader enough information and self-questioning on how to address wear in tribocontacts.

2 The usual approach to consider wear

Wear can occur through different mechanisms that are classified into different categories. The most encountered ones are: abrasion, adhesion, fatigue, and corrosion. Kato and Adachi presented an

interesting diagram that associates the different contact types to the mostly encountered terms and phenomena across literature [3]. They detailed it further in [4]. As can be seen on Figure 1, there is always a deformation state at some point during the wear process. The deformation state is not univocally linked to a type of wear. In this section, the four main types of wear will be discussed along with the associated phenomena. Other types of wear exist through the different scales such as thermal assisted wear, fracture, atomic attrition, etc. However, the rationale behind the study of wear given all along the whole chapter can be applied to all of them.

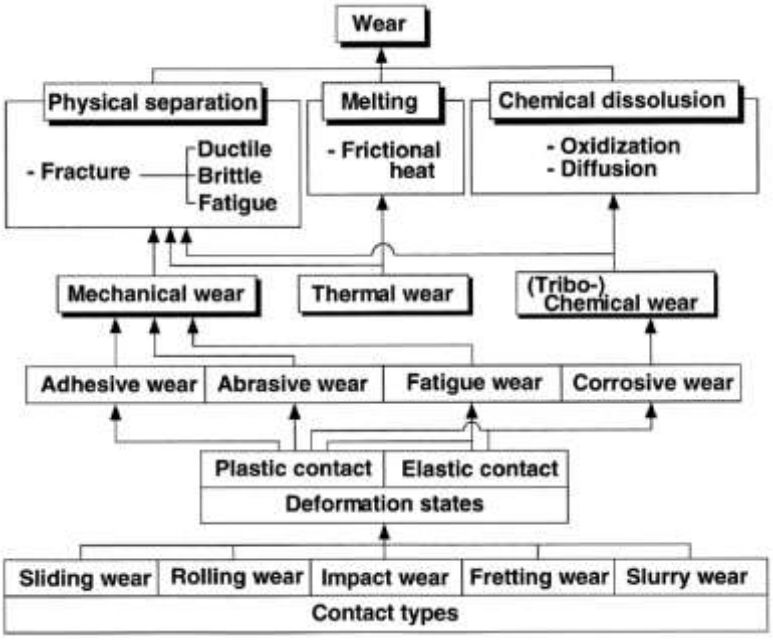


Figure 1 - Descriptive terms linked to different contact types and wear [3]

2.1 Adhesive wear

Adhesive wear is, with abrasion, the mostly encountered wear mode. It results from the creation of junctions between the materials initially in contact (Figure 2). Two cases are encountered [3,10]. Firstly, the interactions can be weak, the interface shear strength remains lower than the yield and rupture strength of the bulk materials. Shear hence happens at the junction and the interface remains. That leads to mild wear. Secondly, the interactions can be strong. In that case, interface turns into bulk cohesive junctions. If the interface shear strength is higher than the yield and rupture strengths of the bulk, shear is located within the bulk of the material. Crack is initiated, then propagates until full failure of the junction. That results in particle creation or material transfer. Particles can exhibit either flake-like or wedge-like morphologies. Eventually, this results in welding, seizure of materials, and severe wear. However, if the transferred material is lubricious, then the wear life of the contact can be very long. Gentle adhesive wear to produce stable lubricious transfer layer is the driving mechanisms in solid lubrication [11–14]. Figure 2 shows and example of transferred film from a solid lubricated contact [11].

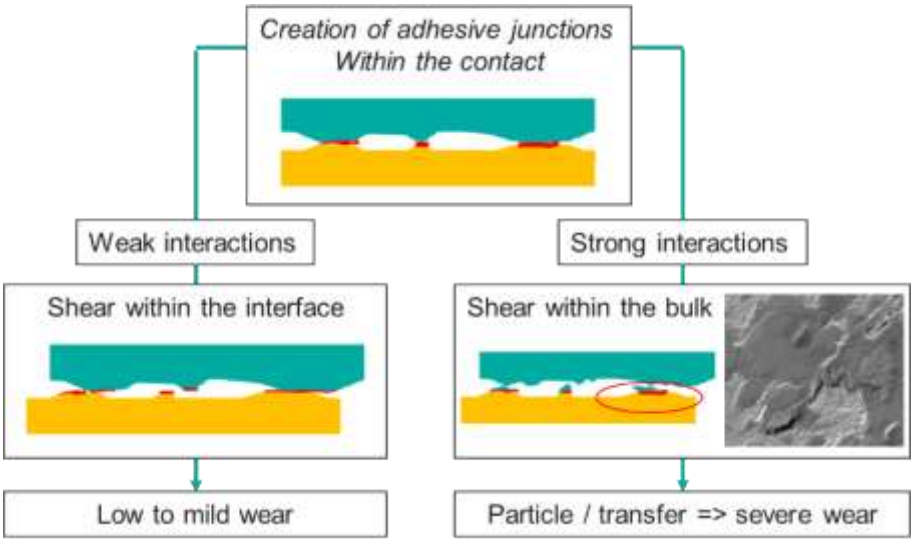


Figure 2 - schematic related to adhesive wear, image of transferred material from [11]

In his review of adhesive wear failures, Podgornik [10] reports four different modes of adhesive failure. Figure 3 shows two of the four morphologies on real surfaces. The four modes are:

- *Scuffing*: it is a localized damage caused by solid phase welding between the sliding interfaces. It involves local plastic deformation, work hardening, and eventually burst of dislocation leading to severe deformation and material removal. There is material transfer between the surfaces, which results in rough and heavily distorted surfaces. Scuffing can be non-uniformly distributed over the surface, and lead to sudden increase in noise and vibrations of the system. Scuffing is often observed in gears applications.
- *Scoring*: similar to scuffing, it is more severe. It is characterized by gross local adhesive transfer. Extrusion of material and particle tearing occurs due to metal/metal contacts and local welding. The surfaces morphology exhibits large and deep grooves due to plastic deformation and material extrusion. Cold-welding [15,16] can lead to scoring.
- *Galling*: associated to metal forming (deep drawing, fine blanking), it is characterized by material transfer to the tool, which in turns induces scratches to metal to be deformed or blanked. ASTM international standard G40 defines it as " ‘‘a form of surface damage arising between sliding solids, distinguished by macroscopic, usually localized, roughening and creations of protrusion rising above the original surface. It often includes material transfer, or plastic flow, or both.’’ It can be combined to abrasive wear.
- *Seizure*: extremely severe case of adhesive wear, the parts cannot be separated without external action to separate them. Cold-welding [15,16] in space mechanism is a good example, forces required to separate the parts can be 2 to 3 times higher than the initial contact load. Creation of gluing interface due to local wear can also lead to seizure [17,18]. Insufficient cooling and/or lubrication in piston/cylinder liner can lead to scuffing and seizure [10,19].

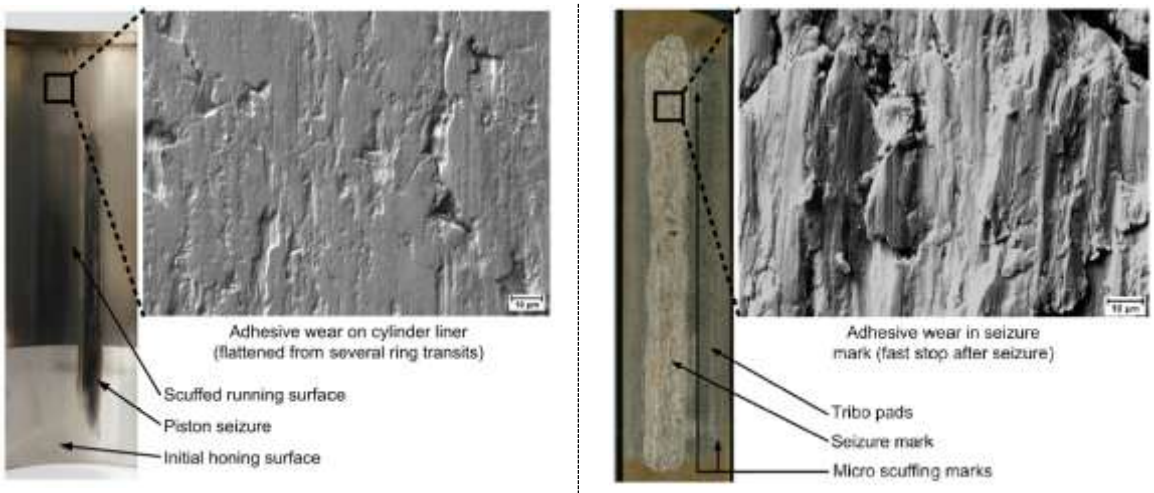


Figure 3 – Liner analysis after tribological test: (a) large overview of the sample showing the seized region and the moderately worn region, (b) magnification of the seized region showing typical morphology of seizure. From [19]

There exist multiple contact mechanics models to estimate adhesion between flat and rough surfaces. They all consider deformation in the elastic domain, but not in plastic domain. Among them are found the Johnson-Kendal-Roberts (JKR), Darjeguin-Muller-Toporov (DMT), and Maugis-Dungdale models [20–22] for flat surfaces, and Fuller & Tabor [23], Persson [24] Rabinovich [25], Rumpf and modified Rumpf [26,27], and Katainen [28] models for rough surfaces. Even in AFM based adhesion measurement in purely elastic domain, transfer to the probe can occur without being detected in the measurement [29]. After proper checking of the probe surface to make sure transfer is limited, the work of adhesion can be calculated with adequate theoretical model (DMT model and Darjeguin approximation in that case).,. In a subsequent study including numerical modeling, the calculated value in combination with the relevant mechanical properties of the simulated material, modeling the experiment allowed to demonstrate the effective particle detachment and that transfer occurs with local plastic deformation of the surface [30]. The recent advancement in numerical modelling now allows to access the driving mechanisms from the junction creation to particle creation [31–33]. Aghababaei et al [31] notably showed that adhesive wear is controlled by three parameters: the size of the asperity contact junction; the work of adhesion of the bulk material; and the maximum elastic strain energy that can be stored at a contact. They were hence able to simulate transitions in adhesive wear mechanisms, and find relevant potentials and analytical model.

To quantify adhesive wear, or at least how fast wear occurs at the whole contact scale, Archard [34] developed a wear law in the 1950s that relates the worn volume (*V*), the normal load (F_n), the sliding distance (*L*), and the hardness of the softer material (*H*). At *H* and F_n constant, the wear law Eq (1) becomes linear with regards to *L*. A coefficient *K* is then identified, and is called wear coefficient. Eq (2) is also encountered, where K* hence has the unit mm^3/Nm and is considered as wear rate.

$$\text{Eq (1).} \quad V = K * \frac{F_n}{H} * L$$

$$\text{Eq (2).} \quad V = K^* * F_n * L$$

First thing to remember before using this model is the seven assumptions to meet to use the Archard approach. As the number of papers using the model without meeting the assumption is growing, here are the assumptions:

#1 The Archard wear model was developed for adhesive wear, in the presence of plastic deformation

#2 The asperities exhibit a spherical geometry, and they are all identical. That means that the contact area between asperities is a disc of radius *a*

#3 The mean contact area remains constant throughout the test. That means that an increase in normal load, implies and increase of the number of contacting asperities. The higher the load, the larger the number of asperities in contact, the larger the mean contact area over the whole contact.

#4 The area of contact is considered as null as soon as the sliding distance equals the diameter of the individual contact (2**a*). Therefore, a new individual contact is created elsewhere inside the contact.

#5 The created wear particles have a lump or layer shape.

#6 Each and every particle created inside the contact during friction is ejected outside the contact area.

#7 All contacts between asperities do not produce wear particles. Only a statistical portion of those contact create particles. A probability factor independent of the particle size (*K* in Eq (1)) hence exist. It lies in the range of 0 to 1.

In practice, determining the wear law of a contact (couple of material rubbing against one another) requires a statistical study to collect a relevant amount of datapoints to draw conclusions. In its study, Archard collected tenths of data points, for each and every contact he studied, as well as data from literature. Several loads have been used, and test have been conducted over different durations. The shortest test was however stopped when the contact was in its steady state regime of friction. Indeed, such model is dedicated to study the evolution of wear over a long-term use of a machinery. Consequently, running-in process are excluded. When studies are presenting wear rates with only a few data points, it should be considered with caution. In this model, deformation mechanisms are not considered. If considered, the wear law might deviate from monotonic variations, as it has been demonstrated by Xu and Persson [35]. The Archard law nonetheless remains quite powerful, it can indeed be verified down to the nanoscale [36,37].

Finally, in adhesive wear, transfer can occur. That means that material is transferred to the counter body, and in a sense, becomes part of it. One can ask itself if measuring wear volume only on the first body makes sense, or if both bodies must be considered. In the study of Sutton et al [38], wear of both bodies is considered. But as transfer occurs, the wear rate of one material is reduced, and as the contact does not fully obey to the Archard law, semi-empirical models and time dependent specific wear rate were introduced.

2.2 Abrasive Wear

Abrasive wear is usually associated with a hard material damaging a softer one during relative motion (rolling and/or sliding) [3,4,39]. Damages can lead to the formation of grooves through purely plastic deformation (Figure 4), in that case the phenomenon is called ploughing, and pile-up of material can be observed on each side of the groove. In this case, particle is not generated during the first pass, it requires multiple cycle of sliding to initiate particle generation. When pile-up is mostly located at the front of the contact, the term wedge-forming mode can be encountered. This mode is most likely assisted by adhesion Both occur with ductile and elastoplastic materials. Finally, cutting can also be associated to abrasive wear (Figure 4), when chip-like ribbon is observed in front of the contact. All can lead to particle detachment.

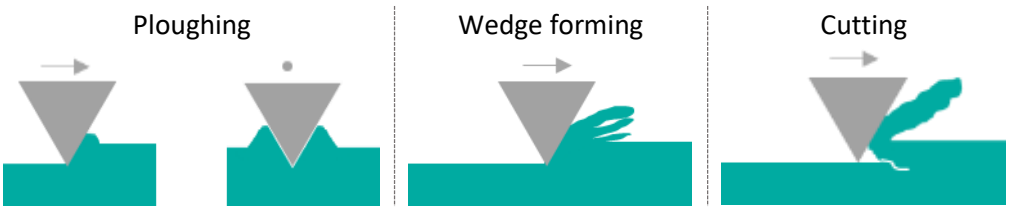


Figure 4 - Schematic of the main mechanisms defining abrasion

Different theoretical models can be found to quantify abrasion. Abrasion, is often described as hard asperities scratching the softer counter body. If such asperity is considered as a cone of half-angle θ, and that the case is ideally plastic, the wear law is defined in Eq (3). That is very similar to the Archard law. K_{ab} is the abrasive wear constant for abrasion of ideally plastic material by a single hard asperity If pile up occurs, the equation must be adjusted to considers the displaced volume. Further detail can be found in [3,40].

$$\text{Eq (3).} \qquad V = \frac{2*tan\theta}{\pi} * \frac{WL}{H} = K_{ab} * \frac{WL}{H}$$

The model and description above are valid for ductile materials. It is worth to mention that it is concerning single asperity. In practice, multiple abrasive spots are located in a contact, leading to a scratched surface during friction. Kato discusses a way to consider the distribution of individual abrasive contacts in the whole area of contact [3]. On brittle materials, abrasion occurs through particle detachment by lateral propagations of cracks in the softer brittle material, at the tip of the contact (Figure 5). The propagation of cracks eventually leads to fracture and particle removal. Fracture toughness K_c is consequently an important parameter that drives abrasion of brittle material. The model of Evans and Marshall[41] is highly encountered.



Figure 5 - Schematic of abrasion in brittle material

$$\text{Eq (4).} \qquad V = \alpha \frac{W^{9/8}}{K_c^{1/2} H^{5/8}} \left(\frac{E}{H}\right)^{4/5} L$$

When abrasion appears in the contact between two bodies initially in contact, it can be called two-body abrasion. If it occurs due to the circulation of a hard particle inside the contact, it is called three-body abrasion. The abrasive mode can switch for two to three-body over the course of friction when a detached particle stays within the contact, or if an external particle gets into it.

2.2.1 Fatigue wear

While abrasive and adhesive wear may occur as soon as the two bodies in contact are put in motion relative to one another, fatigue wear occurs after repeated number of passages of the moving body over the same point of contact [3,4,39]. The repeated passages create weak spots underneath the surface, from which cracks initiate and progressively reach the surface (Figure 6). Eventually a particle is detached. It is important to note that in fatigue wear happens in elastic and elastoplastic contacts [3]. Due to material inhomogeneities, local stress concentration may happen in the material bulk below

the surface, and reach the yield stress. Cycle after cycle of friction/rolling, work hardening or growth of the local stressed domains takes place leading to surface damage overtime. The surface consequently exhibits pitted appearances and debris often have a flake morphology. Fatigue wear is hence sometimes associated to pitting and spalling. Although fatigue wear is often related to rolling motion, it can also be observed in pure sliding contact.

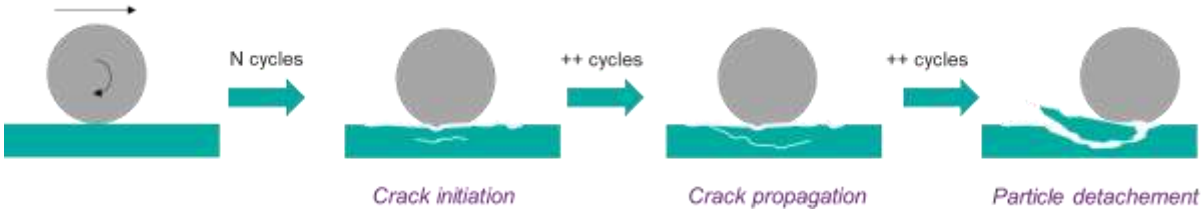


Figure 6 - Schematic of the crack propagation and particle detachment in fatigue wear

Rolling fatigue wear is measured as the number of cycles to reach the ultimate life of the contact [3,39]. The criteria defining a test failure may vary from one application to another. For example, it could be related to a mean torque value, or to an amplitude of variation around its mean value (similar to noise in the torque signal). Numbers of model to express the wear life in rolling contact fatigue relies on the Lundberg-Palmgren theory [3,42,43]. The bearing rings are subjected to N cycles of repeated loading, the probability of survival S is given by Eq (5) where τ_0 is the maximum orthogonal shear stress in the contact, z_0 is the corresponding depth at which the stress occurs, V is the stressed volume in the material. Based on geometric parameters of the bearing and on some simplifications, the life for 10% reliability (90% of the bearing population will endure) can be expressed by Eq (6). where C represents the dynamic load rating, and P the equivalent load on the bearing. The exponent n is equal to 3 for ball bearing, $10/3$ for roller bearing, and 4 for line contacts. The reader is invited to read [42–44] for further models based on Lundberg-Palmgren theory, examples, and discussions. Deterministic models are also discussed in [42].

$$\text{Eq (5).} \qquad ln\left(\frac{1}{S}\right) = A\frac{N^e \tau_0^c V}{z_0^h}$$

$$\text{Eq (6).} \qquad L_{10} = \left(\frac{C}{P}\right)^n$$

A limitation of those models is that they assume a homogeneous description of contact. Some remain statistical, they are based on Weibull statistical strength theory to treat the probability of spalling event occurrence. Local inhomogeneities either in surface, or in volume underneath the surface are not considered [3,42]. Such approaches however remain well accepted in the design of ball bearings [3,43]. To fully understand the mechanisms taking place during rolling contact fatigue, it is of outmost importance to consider local inhomogeneities and subsurface transformations [45]. The subsurface transformations, also called superficial tribological transformations (STT)[4], can lead to grain refinement, change in microstructures, creation of dark etching region (DER) within the material and then white etching areas [45–47]. In Goigoux et al [45], to experimentally simulate the creation of real indent on the bearing races surface, the rolling contact was submitted first to 1 minute of rolling lubricated condition in an open circulation of oil contaminated with hard particles. The samples where then cleaned and submitted to Rolling contact fatigue (RCF) in well lubricated conditions. They hence demonstrated how indent can significantly affect RCF life. In depth insights into the mechanisms leading to fatigue failure are given, from the grain refinement to the crack creation, its propagation, and finally its opening.

Under pure sliding conditions, fatigue wear may also be encountered [3,35,48–52]. In that case, elasticity and plasticity are explicitly considered. The crack initiation is either associated to asperities plastic deformation, surface shear strain, ratchetting effect, or concentration of plastic deformation locally within the bulk, which eventually leads to crack initiation, etc. Nonetheless, consideration of statistically distributed asperities, and statistical shape distribution is needed in some approaches. Such approaches consequently do not consider local homogeneities. Assumption of the existence of initial cracks must be considered in some other models. The crack dimension can be linked to the surface roughness. For sliding contact fatigue, some theoretical approaches are based on the Paris law for fatigue crack growth coupled with Persson's approaches [51], for example. However Paris' Law validity is initially for long cracks rather than small one as encountered in tribological contact [51,53,54].

2.3 Corrosive wear

Corrosion refers to the degradation or transformation of one material and its properties by chemical or electrochemical reaction with the environment. It hence results from a chemical interaction between the environment and the surface of the material that is exposed to it. The reaction is irreversible and it results in a loss of material, or a dissolution of one of the environment compounds/elements in the material. Tribocorrosion is the degradation of material resulting from the combined action of corrosion and mechanical contact stresses (friction and wear) [55,56]. The total wear W_{total} can be expressed as a function of the mechanical wear W_{mech} and corrosion related wear W_{corr_rel}. Three different cases can be seen [56]:

- Case 1: the system is run continuously

$$\text{Eq (7).} \qquad W_{total} = \left(W_{mech} + W_{corr_rel}\right) * t_{operation}$$

- Case 2: the system's operation life is divided into rest and running periods, such as a hip joint

$$\text{Eq (8).} \qquad W_{total} = W_{corr_rel} * t_{rest} + \left(W_{mech} + W_{corr_rel}\right) * t_{running}$$

- Case 3: the system's operation life is divided into rest and running periods in different environment, such as machines functioning outdoors. When the system is running, it can operate in either wet (in the rain) or dry conditions. In the latter case, both mechanical and chemical wear are combined, in the former condition it is admitted that mostly mechanical wear is happening.

$$\text{Eq (9).} \qquad W_{total} = W_{corr_rel} * t_{rest} + \left(W_{mech} + W_{corr_rel}\right) * t_{running\ HR} + W_{corr_rel} * t_{running\ dry}$$

At the end, it is a matter of adding the contribution of mechanical wear W_{mech}, corrosion wear W_{corr}, and corrosion assisted mechanical wear, also known as wear accelerated corrosion, W_{chem} [55,56]. Considering only wear volumes V, it simplifies into Eq (10).

$$\text{Eq (10).} \qquad V_{total} = V_{chem} + V_{mech} + V_{corr}$$

Figure 7 shows the different sources of wear that can interact with corrosion. Corrosion may naturally take place via chemical reaction with the surface and the media, but in passive materials (the most commonly used in tribological contacts) the thin oxide layer existing on the surface slows down the process. As soon as friction takes place, surface deformation and cracks formation quickly degrade the passivation layer. Cracks remains open and debris are free to move inside the contact or in its vicinity. In some cases, such as stainless steels, surface and subsurface tribological transformations (STT) can be observed. STT results in plastically deformed layer that is still part of the bulk, but that is exhibiting

its own microstructure, mechanical properties, and sometimes its own chemical properties. Once the passivation layer is removed, corrosion of athe newly formed surfaces and debris is accelerated. In one hand, corrosion can result in the dissolution of materials with, sometimes, the creation of pits on the surface [57]. That can be accelerated if crack opening exists with the corrosive media entering the cracks. On the other hand, repassivation of the surface occurs to eventually reform the protective layer. If the contact is in a corrosive solution, then debris can be dissolved, leaving the contact in a two bodies tribosystem. However, corrosion can also promote wear. For example, selective corrosion of grain boundaries may occur, which eventually weakens the grain cohesion and facilitates grain detachment from the surface [56]. Dissolution and selective corrosion may also leave localized damage on the surface [57].

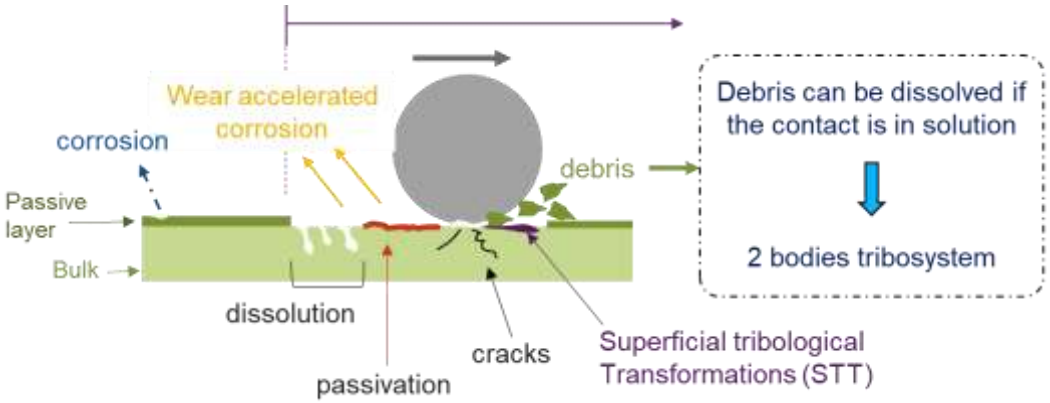


Figure 7 - Schematic of some possible sources of wear interacting with corrosion. Based on [4,55,56,58]

A good example of beneficial tribocorrosion is the creation of a protective passivation at the surface of a AISI440C stainless steel pin sliding against a AISI440C stainless steel plate, in moderate vacuum [59]. Although the Si content in AISI440C is lower than 1%, reaction with the residual water from the moderate vacuum environment with the AISI440C during friction led to the formation of a SiO_x layer which prevented adhesion/welding of the two parts. It also prevented the creation of debris.

As the description framework is given, the next step is the quantification of the different mechanical, chemical, and mechanically assisted chemical wear volumes. As discussed in previous section, plastic deformation systematically occurs during the wear process. Depending on the tribosystem, equations will vary. The reader is invited to read the review from Cao et al [60] where different categories of models are discussed (two-body or three-body contact models, lubricated tribocorrosion model, empirical models, multi-degradation models). Igual Munoz et al [56] are discussing some examples. First, they show that in a system where depassivation occurs by plastic deformation, there is relationship between the anodic current I_a, the depassivation rate R_{dep}, the passivation charge density Q_p, the sliding velocity v_s, the normal force F_n, and the hardness of the surface H. This relationship expressed in Eq (11), k_a is a constant.

$$\text{Eq (11).} \qquad I_a = R_{dep} Q_p = k_a v_s \left(\frac{F_n}{H}\right)^{0.5} Q_p$$

In the case of wear that meet the Archard model, in a mixed lubrication regime (existence of contact between asperity with the fluid circulating in between the asperities in contact), the equation defining the total wear volume from mechanical and chemical wear can be written as follow:

$$\text{Eq (12).} \qquad V_{tot} = k_{mech} \frac{(E')^{0,6556}}{\eta^{0,9685}} . \frac{(F_n)^{1,3129}(v_s)^{0,0315}}{(R')^{1,1473} H} + k_{chem} \frac{M Q_p (E')^{0,3278}}{n F_n \rho \eta^{0,4843}} . \frac{(F_n)^{0,6565}(v_s)^{0,5158}}{(R')^{0,5737} H^{0,5}}$$

E' is the effective Young's modulus of the contact, R' is the effective curvature, η is the fluid viscosity, M is the atomic mass of the metal, F is the Faraday constant, ρ is the metal density, k_{mech} and k_{chem} are calibrated constants coefficient. The calibration has to be done on dedicated tribometer during testing with the metal alloys used in the tribocorrosion study. From Eq (11) and Eq (12), the relationship between chemistry and mechanics is obvious. However, it does not tell how to dissociate and quantify both wear volume (mechanical and chemical). A "straightforward" way to evaluate it consists in performing tribological in electrochemical cells. Then one can either measure only the potential variation during the test, or it can impose a constant potential. When the former approach is chosen, the current necessary to maintain the potential constant is measured all along the test. In that case, Q_p is the integrated value of the excess current measured during the test. Note that the background current must be subtracted first. Hence the wear volume from chemical wear can be calculated. Then, the wear volume due to mechanical wear only is obtained by subtracting the chemical wear volume to the total wear volume (measured after test).

2.4 And now?

Such a bold question can, and should be asked. Most of the definitions and models discussed above are either considering the contact as a whole with specific assumptions (e.g. asperities shape and distribution, ejection of particles), or they describe phenomenon at the local scale. They however do not consider the fact that in reality, at least two to three mechanisms are encountered, at once or successively, in different magnitudes. For example, a contact might first suffer from oxidation, which creates abrasive oxide particles, that then abrade the sliding bodies, to eventually create a layer of material that encompasses compaction and adhesive wear [61]. It is of outmost importance to study the surfaces, their morphologies, and use the classification above as a tool to guide the expertise and define which type of wear happened here and there inside the contact. Then, the researcher, engineer, or technician will know where to look into to better understand what happened, and to improve the tribo-systems.

However, all those studies are based on interrupted test, contact should be opened, and surfaces analyzed. There is a lack of real time analysis of wear, and most of the discussion above assumes that there is no loose material inside the contact. In multi-asperity contact, when a particle detached within the contact area, it is necessarily trapped inside the contact for some time. To fully understand the contact and the "wear dynamic", such trapping should be considered too. The third body concept hence became an interesting tool to describe and investigate the contact while considering all the materials and particles circulating inside and outside the contact.

3 Third body concept in this framework of wear studies

The concept of a third body was first introduced in 1964 [62]. It is defined as a body interposed between two friction surfaces that helps to accommodate speed differences. During the 1970s, the definition was refined, and in 1984, Godet [63] provided the first definition. The third body is an intermediate layer—not necessarily continuous—whose function is to separate the bodies in contact (the first bodies), provide support to transmit forces, and accommodate the relative velocities between the two first bodies (Figure 8). It can be natural (oxides, adsorbates, particles resulting from the degradation of the initial materials, etc.) or artificial, i.e. composed of external elements that come into contact from the outside of the system and that are injected into it (external supply of lubricating powder, gases, oils, etc.). Figure 8 gives example of 3rd body morphologies that can be observed within a contact. In 1990, Berthier [64,65] further extended the definition to include the mechanism (tribosystem) in which the contact is located. It is very important to consider the mechanism because it imposes the contact conditions (normal load, sliding speed), and the tribosystem mechanical properties (stiffness, damping,

degrees of freedom, eigen frequencies, etc.) impacts significantly the contact response, and vice versa [2,66].

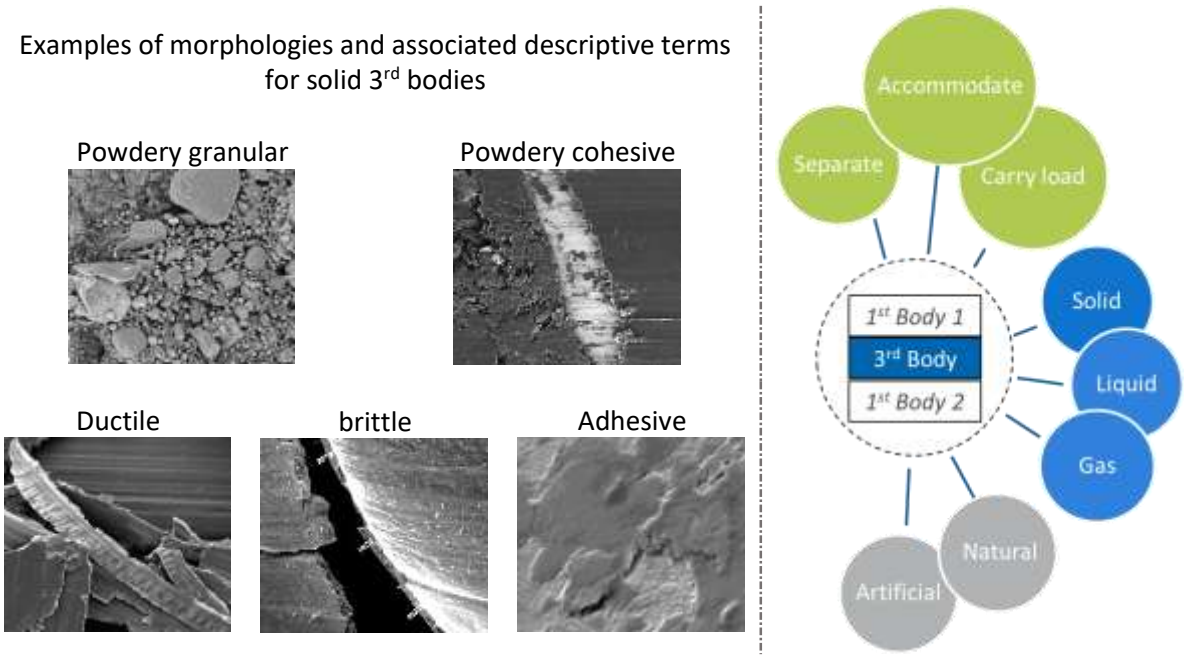


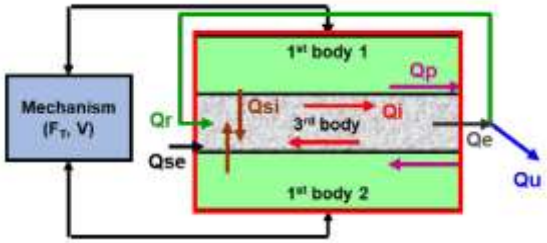
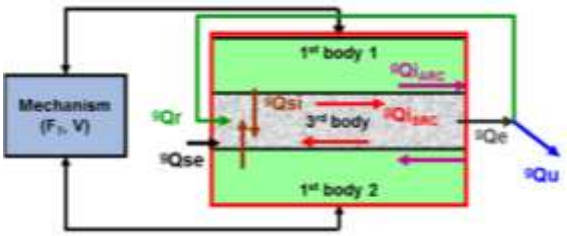
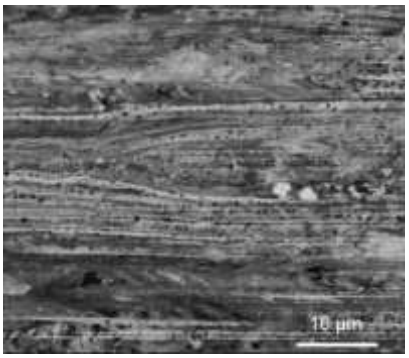
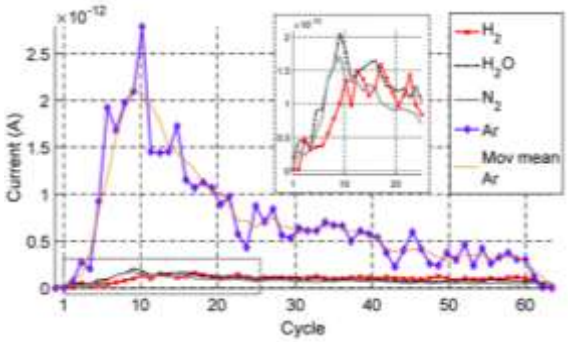
Figure 8 - (Left) Examples of morphologies and descriptive terms that can be associated to them, (right) schematic of the definition of 3rd body

The concept of 3rd body goes farther with the definition of flows of solid particle (Table 1) from its creation within the contact (internal source flow Q_{si}), to its circulation inside the contact (internal flow Q_i), it's ejection (ejection flow Q_e). When ejected, particles can either be definitely ejected (wear flow Q_u) or reenter the contact and recirculate inside it (recirculation flow Q_r). To prove such behavior, testing with transparent sample (sapphire) has been performed [14,65,67]. Post-test analysis of surfaces can also show the footprint of particle circulation within the contact, as shown in Table 1. A flow that is debated is the plastic flow (Q_p) at the surface and subsurface of firsts bodies. This is because it is not a 3rd body yet. However, the presence of plastic deformation often drives the creation of particles, as discussed in the abrasive and adhesive wear modes. The estimation of how extended the surface plastic flow is can be qualitatively evaluated by this last flow. Note also that the source flow can also be external to the contact (Q_{se}), e.g. dust or sand.

Although gas interaction of the contact with the gaseous atmosphere is well known, the gaseous 3rd body flows have been conceptualized similarly to the solid flows, only in 2018 [68]. Desorption and adsorption of gas during friction is well known [12,68–72]. But one can say that during friction, creation of cracks may release gas and hence desorption occurs. The formation of cracks and plastic deformations creates dangling bonds ready to react with the environments once exposed to it (adsorption). However, post-test analysis of the materials shows that the 3rd body that is trapped within the contact (transferred material on the pin, and never exposed directly exposed to the environment) can present a chemical composition that can be obtained only by chemical reactions with the molecules comprising the gaseous environment. For example, the creation of biphasic materials comprising nitrogen, when nitrogen was not present within the materials, but only in the environment [12]. Finally, in the same study, it is discussed that physisorption (physical adsorption without chemical reaction) can occur and significantly drive the friction and wear response of the contact[12]. A comprehensive study of the 3rd body flows can significantly help in understanding the mechanisms taking place within the contact [13,68,73,74]. To fully translate such event in the framework of third body concept, flows have been defined similarly, with exponent "g" added. The gaseous internal source flow has been subdivided into two

sub-flows: the internal source flow with chemical reaction ($^{g}Qi_{src}$) and without chemical reaction ($^{g}Qi_{arc}$). Finally, following gas adsorption and desorption is also an undirect way to detect which of the materials constituting the contact is stressed during friction (the thin layer, the 3rd body, the substrate, etc.) [12]. A mass spectrum obtained during friction test in vacuum and showing desorption of gs during friction is presented in Table 1.

Table 1 - Schematic of solid and gas 3rd body flows inside and outside the contact, with an example of how to identify the existence of one specific flow

Solid 3rd body flows	Gas 3rd body flows [68]
	
▼ Footprint of particle circulation within the contact area of a MoS_2 lubricated contact [75]	▼ Mass spectrum showing desorption of gas during friction, corresponds to $^{g}Q_u$
	

Finally, there exist also sites and accommodations modes that helps categorize where and how the friction accommodations is undertaken within the contact [64,65]. Six sites are defined: the mechanisms S0, the first bodies S1 and S5, the 3rd body in its volume S3, and the interfaces between 1st and 3rd bodies S2 and S4. There are five modes of accommodation: elastic deformation M0, plastic deformation M1, rupture/fracture M2, shear M3, rolling M4.

With such comprehensive description of the contact over the full period of time during which the test is performed, the wear study and description can be comprehensive too, and not restricted to solely abrasive/adhesive/fatigue, etc. All descriptors can be located and distributed within the contact over time, and the particles can be taken into account. This is very important because they can have a significant impact on wear of the material and the system: localization of high surface stress which further enhance wear [74], too high a volume may accelerate wear rather than protect from it [76], insertion of 3rd body into the first bodies to eventually act as a wedge and induce fracture wear [73], induction of vibration propagation [66] and torque noise [77], distribution of stresses within the overall contact and impact clearances [2], lubrication [13,14,78], braking [9,76,79], etc.

4 Understanding the origin of wear

After a test, or following a failure of any system, the first thing that anybody does is to look at the surfaces. To do that, we all look at them at naked eyes, then by using optical microscopes, and eventually scanning electron microscopes (SEM) to better grasp what could have happened. The different concepts discussed in the previous sections are amazing tools to broadly describe the mechanism by which wear and lubrication occurs, and the dynamic of it. They also help in discriminating the magnitude of each of them compared to the others. Such broad schematic of what happens inside the contact, combined with our reading of morphological observations (colors, particle shapes, surface morphologies) then directs the research towards specific domain (e.g tribocorrosion, plasticity, crystallography, fatigue, mechanochemistry) or model (e.g Archard). It also gives insight into the scale to work at in order to find the root mechanisms. Hence, it drives the scientist towards specific analysis tools (SEM, TEM, EBSD, EDS, XPS, Raman, FTIR, ToF-SIMS, AFM, nanoindentation, etc..) to extract the best physical, chemical, and mechanical information to understand the involved mechanisms to finally predict them. It may also drive the choice for dedicated fundamental experiments. Finally, it helps in finding the proper numerical model to better understand, or predict wear. There is need for a strong numerical modelling to visualize/quantify/discriminate the involved mechanisms within the contact and the materials. Discussing the numerical modelling is out of the scope of this chapter. the reader is encouraged to read 3 detailed in depth reviews on the numerical modelling of friction and wear [5,80,81]. Here, two examples are given on how the presented tools can help in understanding the wear mechanisms in a lubricated contact. The reader will note that in that case, there is no mention of wear rate, nor wear life, as the objective of the example is to discuss the fundamental understanding of the origin of wear.

First example, the study of MoS_2 coating wear mechanisms. In the 2010s there was a long discussion in the community regarding the compactness and crystallinity of lubricious coatings. The rule of thumb was “the denser and the harder, the better”. However, it has been demonstrated that a dense fibrous coating could perform better than a “dense amorphous” one. By “amorphous”, it was meant “without long range order across the coating thickness” [59]. The former coating demonstrated plasticization of the coating surface over a very low depth, followed by progressive detachment of nanometric particles that stayed trapped inside the contact, to form an efficient and stable third body layer. The latter demonstrated large propagation of cracks and creation of particles too large to stay trapped inside the contact. The question regarding the reason for such a difference was still remaining: architecture of the coating or a difference in crystalline microstructure? Subsequent studies at the nanoscale [82,83] demonstrated that the architecture and crystalline microstructure was at the origin of the good performance of MoS_2 coating, in the tested conditions. Nanocrystals embedded within an amorphous phase helps preventing propagation of cracks deep inside the coating, and the microstructure further helps deviate the cracks in the shear (friction) direction. Such understanding, based on a first in depth description of the contact morphologies and identified wear and lubricious mechanisms, gave the relevant information to design new efficient coating for the application of interest in those studies [84].

The second example concerns the origin of wear. Is wear driven by mechanics or chemistry? As discussed in the tribocorrosion section, wear can be influenced by corrosion, and vice versa. In both cases, the total wear is significantly worsened or reduced. But, wear can also be moderated by none chemically reactive interaction of the materials and the surrounding molecular environment without impacting the friction coefficient variation. This was observed with MoS_2 sliding against stainless steel in dry nitrogen environment and in vacuum. It is supposed that dry nitrogen molecules adsorb physically on MoS_2, reducing adhesion between the MoS_2 particles themselves, and with the remaining

coating. Friction in dry nitrogen remained in the same order of magnitude than in vacuum, but wear was significantly reduced [12].

5 Quantification of Wear volume?

At the end, from application standpoint, it often comes down to “by how much the parts are worn”, whatever the meaning of wear: lubrication fails by material removal, there is a loss of functional clearances, or degradation of lubricants. The first two cases are relevant to wear and material removal, and eventually to wear rate. The models and concepts discussed above, always refer to material ejected outside the contact to some extent. That means it is often required to measure that volume. There are different approaches to measure it: weight measurement, tactile profilometer, optical techniques. From Ayerdi et al [85], based on in depth review of 541 papers from 2 recognized journals, and over the period of 2014 to 2018, it was shown that 2 approaches are mostly encountered (3D topography, and cross-section profile integration over length (CSIL)), while gravimetric and standards based methods are the least employed (Figure 9). In their study, they focus on the wear volume measurements of friction tracks after linear reciprocating testing. They discuss the ASTM G133-05 and ASTM 775-11 (2017 version) standard, and CSIL technique. They compare the results obtained to those obtained from optical 3D profilometry. Depending on the regularity of the wear track morphology, its length, they show that the wear volume can be overestimated by 106%, and underestimated by 20%, as compared to full optical 3D topography.

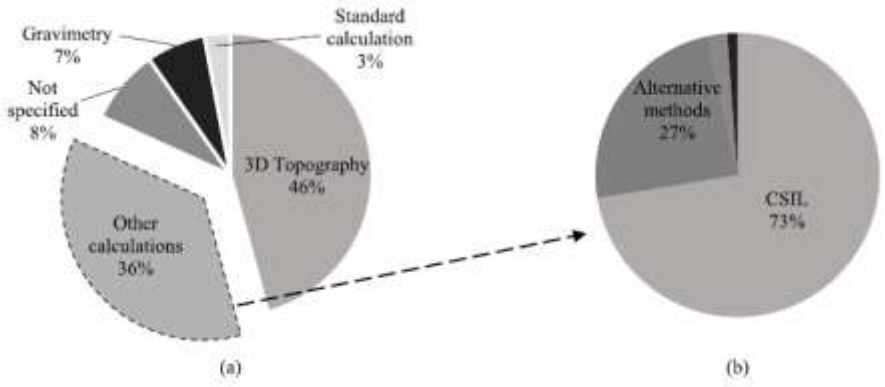
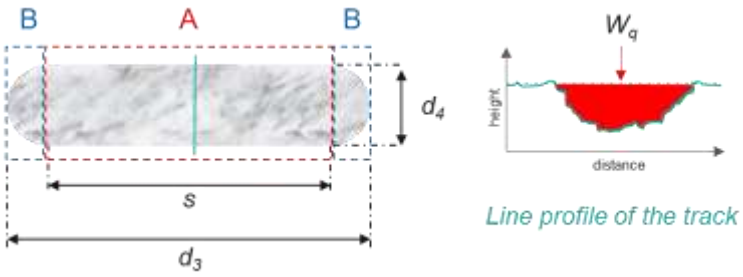


Figure 9 - Distribution of the use of different profilometry characterization techniques for wear volume measurement and calculation, in reciprocating motion tribological test. (a) overview of the main techniques, (b) distribution of the technics categorized as “other calculations”. From [85]

Table 2 gives the equation of the calculation of the wear volumes of the flat sample $W_{v,flat}$, in reciprocating contact. A schematic on which one can visualize what the algebraic numbers refer to is also given. $W_{q,avg}$ in ASTM G133-07 is the average of 3 to six W_q values taken over 3 to 6 profiles equally distributed over the s length. In ASTM 7755-11, the first part of the equation is the volume of both B extremities of the friction track.

Table 2 - Equations for wear volume calculation according to CSIL approach, and to ASTM G133-0 and ASTM 7755-11 (2017). A schematic of a friction track and profile presents the different parameters needed for the calculations.



CSIL	ASTM G133-05	ASTM 7755-11 (2017)
$W_{v,flat} = W_q.S$	$W_{v,flat} = W_{q,avg}.S$	$W_{v,flat} = \frac{\pi d_4^2 (d_3 - s)^2}{64} * \frac{1}{R} + W_q.S$

To reduce the error in the volume estimation, Ayerdi [85] proposed to mix both standards and to not consider the most irregular part of track extremity while defining the limit of the B regions. Hence, they managed to reduce the most extreme error of 106% of the studied cases, down to 17%. Pawel 2025 [86] also discussed the limitations of ASTM 7755-11, just like Ayerdi but for small track length. They also compared the errors with the white light interferometry (WLI). They proposed a slight adjustment of the location of the profiles to minimize the error. They obtained a deduction of average error from 13.9% down to 4.5%. It is worth to note, that they report that white WLI gives similar results than AFM based topography.

Although mentioning the optical techniques are more suitable, Ayerdi et al [85] stated that the accuracy of optical technics is subjected to the instruments precisions and specifications, the parameters used, etc. In fact, there are uncertainties in the measurement of surface topographical features with optical profilometry. Those uncertainties can vary from one technique to another. The reader can find in depth discussion, uncertainties evaluation, and examples in [87,88]. Finally, an uncertainty calculation has also been performed for gravimetric measurement, on reciprocating test [89].

Similar approaches exist for pin-on-disc tests in continuous rotational modes. The recent study of Maculotti [90] is a good example combining uncertainty calculation and surface topography methods in wear volume evaluation of pin-on-disc test. The study also focuses only on the flat sample. They report performing the evaluation on the disc samples as per the ASTM G99 standard that suggest to report wear of the disc and the pin separately, rather than as one value of both contributions. The authors also reported that gravimetric (samples weighing) and volumetric samples (stylus profilometry here) are suggested for the wear volume evaluation of pin-on-disc test, from the same standard. However, the gravimetric method is not adapted to low wear contacts, and it does not give, nor differentiate plastic deformed area such as pile-up from the groove. Stylus profilometry brings more information and allow to differentiate the different regions of the friction track and its surroundings. Hence, depending on the application and their own definition of wear, one may consider specific region grooves, the pile-up on the edge of the track, or both. The approach, and the possible errors, are discussed in terms of surface morphology. Coherence scanning interferometer has been used alongside contact stylus. 4 to 8 profiles were extracted for calculations.

However, two questions remain: should one consider all the track or only a portion of it? Both ball and plate samples are to be considered, or is one sufficient to assess wear? To have a contact in the first place, two bodies are necessary. Both can suffer from wear damage, so how to consider it properly? It

seems reasonable to consider both when estimating the wear or damaged volume depending on the application and the definition of wear. Here the definition will remain as damaged volumes (that includes abrasive or adhesive wear resulting grooves, transfer films, particles remaining inside the contact, etc.). Particles definitively ejected outside the contact at track extremities (on both plate and pin) are not considered. Sutton et al [38] developed an Archard and Preston based model that couples wear from both bodies pin (and plate), and that considers a time dependency of the wear laws. Qu et al [91] discussed the fact that in friction, not all sliders are a ball, and not every worn region on the ball, or pin, is perfectly circular. Consequently, relying on the measurement of the diameter of the scar on the ball/pin, as suggested in ASTM G99, is not fully relevant. A calculation taking into consideration 2 curvatures has been proposed, giving more reliable results. Schmitz et al [89] also considered the pin in there calculation of wear through gravimetric approach.

Cornuault et al. [92] adopted a different approach in the calculation of wear. They considered both samples and measured the total volume loss of both plate and pin samples. They used 3D profilometry on both samples. As shown in Figure 10, on the plate sample only a portion of the friction track is considered, at least half of it. Then the topography is levelled and the mean plane of the pristine surface is put at zero. All positive and negative volumes are considered. On the pin, the overall spherical geometry is removed through quadratic levelling. The resulting mean plane of the pristine region is put at zero. Hence, the wear scar becomes a hole. Positive and negative volumes are also considered in the calculation of wear. The total wear volume was then calculated via Eq (13). With this approach, the authors showed cases where the total wear volume of two different contact could be similar although the wear of plate and pin are very different respectively. Looking solely to the plate would have led to wrong conclusions. Considering both samples is consequently very important.

Eq (13). $$W_{tot} = W_{plate} + W_{Ball} = \frac{V_p^- - V_p^+}{2dN_{cycle}} + \frac{V_b^- - V_b^+}{4N_{cycle}}$$

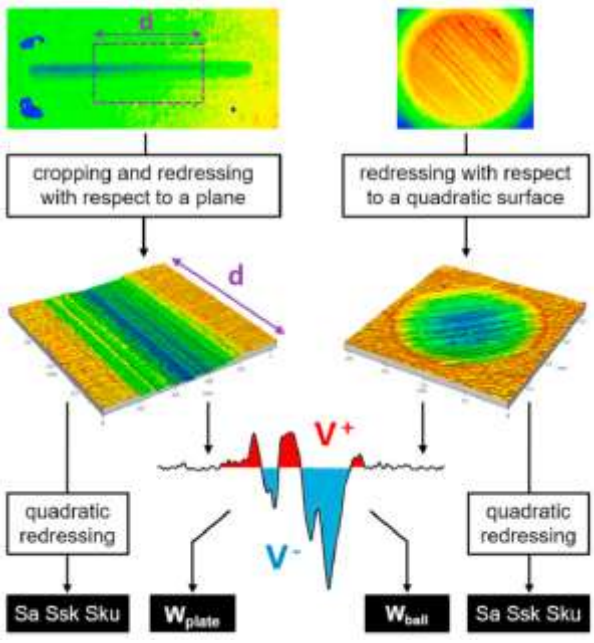


Figure 10 – Schematics of data from 3D optical profilometry to calculate wear rates. From [92]

6 Conclusion

Throughout this chapter, wear has been addressed from the perspective of distinct or combined phenomena, through qualitative experimental descriptions or analytical models. Definitions have thus

been provided (abrasive wear, adhesive wear, fatigue wear, etc.), concepts presented (e.g. third body concept), and discussed. It has been demonstrated that wear cannot be reduced to a volume of worn material, or to a qualitative description of surface morphology. Mastering wear—whether to prevent it or, conversely, to utilize it for lubrication—requires an in-depth understanding of the mechanical, chemical, and physical mechanisms taking place at the system or material levels. The study of wear requires the use of numerous analytical techniques and, at times, numerical models. It is important for anyone facing a wear problem to use the tools presented in this chapter as a means of framing their study to guide them through the necessary additional analyses. Only then a detailed understanding of the mechanisms can be reached, and even their quantification. Finally, let us remember that wear is a system response, not a material property. All analytical models have assumptions to be met, and measuring the volume of wear requires a clear definition of wear itself, as well as a thorough understanding of the limitations of the machines and standards used.

7 References

(1) Bayer, R. G. Mechanical Wear Prediction Prevention. *Strain* **1995**, *31* (3), 115. https://doi.org/https://doi.org/10.1111/j.1475-1305.1995.tb00971.x.

(2) Kohen, I.; Play, D.; Godet, M. Effect of Machine Rigidity or Degrees of Freedom on the Load-Carrying Capacity of Wear Debris. *Wear* **1980**, *61* (2), 381–384. https://doi.org/10.1016/0043-1648(80)90300-2.

(3) Kato, K.; Adachi, K. Chap 7 _ Wear Mechanisms. In *Modern Tribology Handbook, Two Volume Set*; Mechanics & Materials Science; CRC Press, 2000. https://doi.org/doi:10.1201/9780849377877.ch7.

(4) Stachowiak, G. W. *Wear - Materials, Mechanisms and Practice*; John Wiley & Son, Ltd, Chichester, West Sussex, England, 2013; Vol. 53. https://doi.org/10.1017/CBO9781107415324.004.

(5) Pastewka, L.; Vakis, A. I.; Aghababaei, R.; Almqvist, A.; Carbone, G.; Chandross, M.; Dini, D.; Eder, S. J.; Ehrich, H. J.; Ewen, J. P.; Menga, N.; Molinari, J.; Moras, G.; Nicola, L.; Paggi, M.; Putignano, C.; Scaraggi, M.; Yastrebov, V. A.; Müser, M. H. Modeling in Tribology: Recent Advances, Applications, and Open Questions. *Tribol. Int.* **2025**, *218*, 111326. https://doi.org/10.1016/j.triboint.2025.111326.

(6) Holmberg, K.; Erdemir, A. Influence of Tribology on Global Energy Consumption , Costs and Emissions. *Friction* **2017**, *5* (3), 263–284.

(7) Grigoratos, T.; Martini, G. Brake Wear Particle Emissions: A Review. *Environ. Sci. Pollut. Res.* **2015**, *22* (4), 2491–2504. https://doi.org/10.1007/s11356-014-3696-8.

(8) Briatte, M.; Mege-revil, A.; Desplanques, Y.; Parrens, C.; Santacreu, P. Relationships between Third Body Flows , Load-Bearing Mechanisms and Particle Emissions in Automotive Braking. *Wear* **2023**, *524–525* (April), 204855. https://doi.org/10.1016/j.wear.2023.204855.

(9) Briatte, M.; Mege-revil, A.; Desplanques, Y.; Santacreu, P. Effect of the Microstructure of Martensitic Stainless Steel Discs on Wear Processes and Particle Emission in Automotive Braking. *Wear* **2025**, *571* (January), 205825. https://doi.org/10.1016/j.wear.2025.205825.

(10) Podgornik, B. Adhesive Wear Failures. *J. Fail. Anal. Prev.* **2022**, *22* (1), 113–138. https://doi.org/10.1007/s11668-021-01322-4.

(11) Colas, G.; Saulot, A.; Descartes, S.; Michel, Y.; Berthier, Y. Double Transfer Experiments To Highlight Design Criterion for Future Self-Lubricating Materials. In *Conference proceedings of*

the 16th European Space Mechanisms & Tribology Symposium; Bilbao, Spain, 2015.

(12) Colas, G.; Saulot, A.; Bouscharain, N.; Godeau, C.; Michel, Y.; Berthier, Y. How Far Does Contamination Help Dry Lubrication Efficiency? *Tribol. Int.* **2013**, *65*, 177–189. https://doi.org/10.1016/j.triboint.2012.12.011.

(13) Colas, G.; Saulot, A.; Godeau, C.; Michel, Y.; Berthier, Y. Decrypting Third Body Flows to Solve Dry Lubrication Issue - MoS2 Case Study under Ultrahigh Vacuum. *Wear* **2013**, *305* (1–2), 192–204. https://doi.org/10.1016/j.wear.2013.06.007.

(14) Singer, I. L.; Dvorak, S. D.; Wahl, K. J.; Scharf, T. W. Role of Third Bodies in Friction and Wear of Protective Coatings Role of Third Bodies in Friction and Wear of Protective Coatings. *J. Vac. Sci. Technol. A* **2003**, *21* (5), 232–240. https://doi.org/10.1116/1.1599869.

(15) Merstallinger, A.; Holzbauer, R.; Bamsey, N. Cold Welding in Hold down Points of Space Mechanisms Due to Fretting When Omitting Grease. *Lubricants* **2021**, *9* (8). https://doi.org/10.3390/lubricants9080072.

(16) Merstallinger, A.; Sales, M.; Semerad, E. *ESA STM-279_Assessment of Cold Welding between Separable Contact Surfaces Due to Impact and Fretting under Vacuum*; ESA Communication Production Office, 2009.

(17) Colas, G.; Cornuault, P.-H.; Michel, Y.; Petre Bordenave, R. Fretting Wear_Lubrication of Initially Worn Parts through Tribo-Induced Anchorage of PTFE in Wear Scars, and Tribochemical Creation of Graphene Oxide. *Wear* **2023**, *524–525*, 204882.

(18) Colas, G.; Petre-bordenave, R.; Michel, Y.; Cornuault, P. Freting Wear Anomaly of Final CubeSat Ejection Tests : Expertise , Solution Testing ,and Lessons Learnt. In *20th ESMATS*; 2023.

(19) Pusterhofer, M.; Summer, F.; Wuketich, D.; Grün, F. Development of a Model Test System for a Piston Ring / Cylinder Liner-Contact with Focus on Near-to-Application Seizure Behaviour. *Lubricants* **2019**, *7* (104), 1–12. https://doi.org/10.3390/lubricants7120104.

(20) Johnson, K. L. Mechanics of Adhesion. *Tribol. Int.* **1998**, *31* (8), 413–418. https://doi.org/10.1016/S0301-679X(98)00060-7.

(21) Maugis, D. Adhesion of Spheres: The JKR-DMT Transition Using a Dugdale Model. *J. Colloid Interface Sci.* **1992**, *150* (1), 243–269. https://doi.org/10.1016/0021-9797(92)90285-T.

(22) Grierson, D. S.; Flater, E.; Carpick, R. W. Accounting for the JKRDMT Transition in Adhesion and Friction Measurements with Atomic Force Microscopy. *At. Force Microsc. Adhes. Stud.* **2005**, *3* (5), 291–311. https://doi.org/10.1163/1568561054352685.

(23) Fuller, K. N. G.; Tabor, D. The Effect of Surface Roughness on the Adhesion of Elastic Solids. *Proceeding R. Soc. pf London A* **1975**, *345*, 327–342. https://doi.org/10.1098/rspa.1983.0054.

(24) Persson, B. N. J.; Tosatti, E. The Effect of Surface Roughness on the Adhesion of Elastic Solids. *J. Chem. Phys.* **2001**, *115* (12), 5597–5610. https://doi.org/10.1063/1.1398300.

(25) Rabinovich, Y. I.; Adler, J. J.; Ata, A.; Singh, R. K.; Moudgil, B. M. Adhesion between Nanoscale Rough Surfaces: I. Role of Asperity Geometry. *J. Colloid Interface Sci.* **2000**, *232* (1), 10–16. https://doi.org/10.1006/jcis.2000.7167.

(26) Laitinen, O.; Bauer, K.; Niinimäki, J.; Peuker, U. A. Validity of the Rumpf and the Rabinovich Adhesion Force Models for Alumina Substrates with Nanoscale Roughness. *Powder Technol.* **2013**, *246*, 545–552. https://doi.org/10.1016/j.powtec.2013.05.051.

(27) Jiang, T.; Zhu, Y. Measuring Graphene Adhesion Using Atomic Force Microscopy with a

Microsphere Tip. *Nanoscale* **2015**, *7* (24), 10760–10766. https://doi.org/10.1039/c5nr02480c.

(28) Katainen, J.; Paajanen, M.; Ahtola, E.; Pore, V.; Lahtinen, J. Adhesion as an Interplay between Particle Size and Surface Roughness. *J. Colloid Interface Sci.* **2006**, *304* (2), 524–529. https://doi.org/10.1016/j.jcis.2006.09.015.

(29) Pajovic, S.; Colas, G.; Saulot, A.; Renouf, M.; Filleter, T. Work of Adhesion Measurements of MoS2 Dry Lubricated 440C Stainless Steel Tribological Contacts. *Adv. Eng. Mater.* **2017**, *1700423*, 1700423. https://doi.org/10.1002/adem.201700423.

(30) Colas, G.; Pajovic, S.; Saulot, A.; Renouf, M.; Cameron, P. Adhesion Measurements in MoS2 Dry Lubricated Contacts to Inform Predictive Tribological Numerical Models: Comparison Between Laboratory-Tested Samples and Ball Bearings From The NIRISS Mechanism. In *Conference proceedings of the 17th European Space Mechanisms & Tribology Symposium*; Hatfiel, UK, 2017.

(31) Aghababaei, R.; Warner, D. H.; Molinari, J. Critical Length Scale Controls Adhesive Wear Mechanisms. *Nat. Commun.* **2016**, *7*, 1–8. https://doi.org/10.1038/ncomms11816.

(32) Zhang, H.; Goltsberg, R.; Etsion, I. Modeling Adhesive Wear in Asperity and Rough Surface Contacts : A Review. *Materials (Basel).* **2022**, *15*, 6855.

(33) Aghababaei, R.; Zhao, K. Micromechanics of Material Detachment during Adhesive Wear : A Numerical Assessment of Archard ' s Wear Model. *Wear* **2021**, *476*, 203739. https://doi.org/10.1016/j.wear.2021.203739.

(34) Archard, J. F. Contact and Rubbing of Flat Surfaces. *J. Appl. Phys.* **1953**, *34*, 981–988. https://doi.org/10.1063/1.1721448.

(35) Xu, R.; Persson, B. N. J. Sliding Wear : Role of Plasticity. *Tribol. Lett.* **2025**, *73*, 1–18. https://doi.org/10.1007/s11249-025-02044-6.

(36) Noël, O.; Vencl, A.; Mazeran, P.-E. Exploring Wear at the Nano-Scale with the Circular Mode Atomic Force Microscopy. *Beilstein J. Nanotechnol.* **2017**, *8*, 2662–2668.

(37) Vencl, A.; Mazeran, P.-E.; Bellafkih, S.; Noël, O. Assessment of Wear Behaviour of Copper-Based Nanocomposite at the Nanoscale. *Wear* **2018**, *414–415*, 212–218.

(38) Stewart, D. C. S. G. L. D. A Functional Form for Wear Depth of a Ball and a Flat Surface. *Tribol. Lett.* **2014**, *53*, 173–179. https://doi.org/10.1007/s11249-013-0254-3.

(39) Martini, A. *Introduction to Tribology for Engineers*; Independently published, 2022.

(40) Hokkirigawa, K.; Kato, K. An Experimental and Theoretical Investigation of Ploughing , Cutting and Wedge Formation during Abrasive Wear. *Tribol. Int.* **1988**, *21* (1), 51–57.

(41) Evans, A. G.; Marshall, D. B. Wear Mechanisms in Ceramics. In *Fundamentals of friction and wear of materials*; Rigney, D. A., Ed.; American Society of Metals, 1981.

(42) Sadeghi, F.; Jalalahmadi, B.; Slack, T. S.; Raje, N.; Arakere, N. K. A Review of Rolling Contact. *J. Tribol.* **2009**, *131* (October), 1–14. https://doi.org/10.1115/1.3209132.

(43) Harris, T. A.; Kotzalas, M. N. *Rolling Bearing Analysis 5th Edition - 2 Volume Set*; CRC Press, 2006.

(44) Zaretsky, E. V. *Rolling Bearing Life Prediction , Theory , and Application*; 2016.

(45) Goigoux, A.; Cazottes, S.; Biboulet, N.; Ville, F.; Douillard, T.; Dubois, P. E.; Sidoroff, C. Surface-Initiated Rolling Contact Fatigue on a Dent : Microstructural Evolutions through Failure Mechanism. *Acta Mater.* **2024**, *277*, 120201. https://doi.org/10.1016/j.actamat.2024.120201.

(46) Thiercelin, L.; Cazottes, S.; Merino, P.; Saulot, A.; Lebon, F. Mechanical White Etching Layer Formation Kinetics in Pearlitic Steels : A Phenomenological Model Based on Microstructural Characterization. *Wear* **2023**, *514–515* (October 2022), 204585. https://doi.org/10.1016/j.wear.2022.204585.

(47) Wang, H. H.; Wang, W. J.; Han, Z. Y.; Wang, Y.; Ding, H. H.; Lewis, R.; Lin, Q.; Liu, Q. Y.; Zhou, Z. R. Wear and Rolling Contact Fatigue Competition Mechanism of Different Types of Rail Steels under Various Slip Ratios. *Wear* **2023**, *522* (September 2022), 204721. https://doi.org/10.1016/j.wear.2023.204721.

(48) Li, Y.; Xie, G.; Sun, X.; Jingcao, C.; Wu, X. A Review on Fretting Wear / Fatigue Behavior , Protective Measures , and Application Examples of Typical Alloy Materials. *J. Eng. Tribol.* **2025**, *239* (10), 1261–1290. https://doi.org/10.1177/13506501241313249.

(49) Heilmann, P.; Rigney, D. A. Experimental Evidence for Fatigue During Sliding Wear. *Metall. Trans. A* **1981**, *12A*, 686–688.

(50) Persson, B. J.; Xu, R.; Miyashita, N. Rubber Wear : Experiment and Theory. *J. Chem. Phys.* **2025**, *162*, 074704. https://doi.org/10.1063/5.0248199.

(51) Ciavarella, M. Wear Due to Fatigue Initiation. *Tribol. Int.* **2025**, *207*, 110592. https://doi.org/10.1016/j.triboint.2025.110592.

(52) Tan, Y.; Zhang, L.; Hu, Y. A Wear Model of Plane Sliding Pairs Based on Fatigue Contact Analysis of Asperities. *Tribol. Trans.* **2015**, *58* (1), 148–157. https://doi.org/10.1080/10402004.2014.956907.

(53) Pugno, N.; Ciavarella, M.; Cornetti, P.; Carpinteri, A. A Generalized Paris ' Law for Fatigue Crack Growth. *J. Mech. Phys. Solids* **2006**, *54*, 1333–1349. https://doi.org/10.1016/j.jmps.2006.01.007.

(54) Carpinteri, A.; Montagnoli, F. Scaling and Fractality in Subcritical Fatigue Crack Growth : Crack-Size Effects on Paris ' Law and Fatigue Threshold. *Fatigue Fract. Eng. Mater. Struct.* **2020**, *43*, 788–801. https://doi.org/10.1111/ffe.13184.

(55) Richard, C.; Geringer, J. Tribocorrosion. **2019**, *33* (0).

(56) Igual Munoz, A.; Espallargas, N.; Mischler, S. *Tribocorrosion*; Springer Cham, 2020. https://doi.org/https://doi.org/10.1007/978-3-030-48107-0.

(57) Wang, Z. Decline in Pitting Corrosion Resistance of 316 L Stainless Steel Induced by Cr- Depleted Layer during Tribocorrosion. *npj Mater. Degrad.* **2025**, 1–13. https://doi.org/10.1038/s41529-025-00569-8.

(58) Takadoum, J. *Matériaux et Surfaces En Tribologie*; Lavoisier, H.-, Ed.; 2007.

(59) Colas, G.; Saulot, A.; Regis, E.; Berthier, Y. Investigation of Crystalline and Amorphous MoS2 Based Coatings: Towards Developing New Coatings for Space Applications. *Wear* **2015**, *330–331*, 448–460. https://doi.org/10.1016/j.wear.2015.01.011.

(60) Cao, S.; Mischler, S. Modeling Tribocorrosion of Passive Metals – A Review. *Curr. Opin. Solid State Mater. Sci.* **2018**, *22* (4), 127–141. https://doi.org/10.1016/j.cossms.2018.06.001.

(61) Barlemont, S.; Laffont, P.; Daudin, R.; Lenain, A.; Colas, G.; Cornuault, P. Strong Dependency of the Tribological Behavior of CuZr-Based Bulk Metallic Glasses on Relative Humidity in Ambient Air. *Friction* **2023**, *11* (5), 785–800.

(62) Caubet, J. J. *Théorie et Pratique Industrielle Du Frottement*, Dunod Pa.; Dunod Paris, T. P., Ed.;

1964.

(63) Godet, M. The Third-Body Approach: A Mechanical View of Wear. *Wear* **1984**, *100* (1–3), 437–452. https://doi.org/10.1016/0043-1648(84)90025-5.

(64) Berthier, Y. Experimental Evidence for Friction and Wear Modelling. *Wear* **1990**, *139* (1), 77–92. https://doi.org/10.1016/0043-1648(90)90210-2.

(65) Berthier, Y. Third-Body Reality - Consequences and Use of the Third-Body Concept to Solve Friction and Wear Problems. In *Wear - Materials, Mechanisms and Practice*; 2005; pp 291–317.

(66) Renouf, M.; Nhu, V.-H.; Saulot, A.; Massi, F. First-Body Versus Third-Body: Dialogue Between an Experiment and a Combined Discrete and Finite Element Approach. *ASME J. Tribol.* **2014**, *136* (2), 021104. https://doi.org/10.1115/1.4026062.

(67) Descartes, J. M. S. S. Third Body Behavior During Dry Sliding of Cold-Sprayed Al-Al2O3 Composites : In Situ Tribometry and Microanalysis. *Tribol. Lett.* **2014**, *54* (191–206), 191–206. https://doi.org/10.1007/s11249-014-0326-z.

(68) Colas, G.; Saulot, A.; Philippon, D.; Berthier, Y.; Léonard, D. Tribochemical Competition within a MoS2/Ti Dry Lubricated Macroscale Contact in Ultrahigh Vacuum: A Time of Flight Secondary Ion Mass Spectrometry Investigation. *ACS Appl. Mater. Interfaces* **2018**, *10* (23), 20106–20119. https://doi.org/10.1021/acsami.8b02999.

(69) Gouider, M.; Berthier, Y.; Jacquemard, P.; Rousseau, B.; Bonnamy, S.; Estrade-Szwarckopf, H. Mass Spectrometry during C/C Composite Friction: Carbon Oxidation Associated with High Friction Coefficient and High Wear Rate. *Wear* **2004**, *256* (11–12), 1082–1087. https://doi.org/10.1016/S0043-1648(03)00534-9.

(70) Kasem, H.; Bonnamy, S.; Rousseau, B.; Estrade-Szwarckopf, H.; Berthier, Y.; Jacquemard, P. Interdependence between Wear Process, Size of Detached Particles and CO2production during Carbon/Carbon Composite Friction. *Wear* **2007**, *263* (7-12 SPEC. ISS.), 1220–1229. https://doi.org/10.1016/j.wear.2007.01.077.

(71) Nevshupa, R. A.; De Segovia, J. L. Outgassing from Stainless Steel under Impact in UHV. *Vacuum* **2002**, *64* (3–4), 425–430. https://doi.org/10.1016/S0042-207X(01)00345-1.

(72) Nevshupa, R. A.; Roman, E.; De Segovia, J. L. Contamination of Vacuum Environment Due to Gas Emission Stimulated by Friction. *Tribol. Int.* **2013**, *59*, 23–29. https://doi.org/10.1016/j.triboint.2012.07.009.

(73) Champagne, M.; Renouf, M.; Berthier, Y. Modeling Wear for Heterogeneous Bi-Phasic Materials Using Discrete Elements Approach. *J. Tribol.* **2014**, *136* (2), 021603. https://doi.org/10.1115/1.4026053.

(74) Bouillanne, O.; Mollon, G.; Saulot, A.; Descartes, S.; Serres, N. Wear in Progress : How Third Body Flow Controls Surface Damage. *Tribol. Lett.* **2024**, *72* (3), 1–19. https://doi.org/10.1007/s11249-024-01875-z.

(75) Colas, G. Utilisation Raisonnée de Contaminants Pour Caractériser La Rhéologie Des 1ers et 3ème Corps Solides : Application à La Tribologie En Ambiances Spatiales, INSA de Lyon, 2013. https://tel.archives-ouvertes.fr/tel-00961216/.

(76) Briatte, M.; Mege-revil, A.; Desplanques, Y.; Parrens, C.; Santacreu, P. Relationships between Third Body Flows, Load-Bearing Mechanisms and Particle Emissions in Automotive Braking. *Wear* **2023**, *524–525* (April), 204855. https://doi.org/10.1016/j.wear.2023.204855.

(77) Sicre, J.; Michel, Y.; Videira, E.; Nicollet, L.; Baud, D. PGM-HT as RT/Duroïd 5813 Replacement?

Lifetime Results on STD Earth Scanning Sensor and Polder Bearing Shaft. *Proc. 13th Eur. Sp. Mech. Tribol. Symp. - ESMATS 2009 (ESA SP-670)* **2009**, *ESA SP 670* (September).

(78) Bouchot, A.; Ferrieux, A.; Debayle, J.; Mollon, G.; Descartes, S. Image Processing Applied to Tribological Dry Contact Analysis. *Wear* **2021**, *476* (February), 203748. https://doi.org/10.1016/j.wear.2021.203748.

(79) Thévenot, M.; Brunel, J.; Brunel, F.; Briatte, M.; Desplanques, Y.; Dufrénoy, P. Identification of Particle Emission Mechanisms during Dry Friction with Thermomechanical Operando Monitoring. *Wear* **2025**, *570* (September 2024), 205974. https://doi.org/10.1016/j.wear.2025.205974.

(80) Renouf, M.; Massi, F.; Fillot, N.; Saulot, A. Numerical Tribology of a Dry Contact. *Tribol. Int.* **2011**, *44* (7–8), 834–844. https://doi.org/10.1016/j.triboint.2011.02.008.

(81) Vakis, A. I.; Yastrebov, V. A.; Scheibert, J.; Nicola, L.; Dini, D.; Minfray, C.; Almqvist, A.; Paggi, M.; Lee, S.; Limbert, G.; Molinari, J. F.; Anciaux, G.; Aghababaei, R.; Restrepo, S. E.; Papangelo, A.; Cammarata, A.; Nicolini, P.; Putignano, C.; Carbone, G.; Stupkiewicz, S.; Lengiewicz, J.; Costagliola, G.; Bosia, F.; Guarino, R. Modeling and Simulation in Tribology across Scales : An Overview. *Tribol. Int.* **2018**, *125*, 169–199. https://doi.org/10.1016/j.triboint.2018.02.005.

(82) Colas, G.; Serles, P.; Saulot, A.; Filleter, T. Strength Measurement and Rupture Mechanisms of a Micron Thick Nanocrystalline MoS2 Coating Using AFM Based Micro-Bending Tests. *J. Mech. Phys. Solids* **2019**, *128*, 151–161. https://doi.org/10.1016/j.jmps.2019.04.007.

(83) Serles, P.; Sun, H.; Colas, G.; Tam, J.; Nicholson, E.; Wang, G.; Howe, J.; Saulot, A.; Singh, C. V.; Filleter, T. Structure-Dependent Wear and Shear Mechanics of Nanostructured MoS<inf>2</Inf> Coatings. *Adv. Mater. Interfaces* **2020**, *7* (14). https://doi.org/10.1002/admi.201901870.

(84) Serles, P.; Nicholson, E.; Tam, J.; Barri, N.; Chemin, J. B.; Wang, G.; Michel, Y.; Singh, C. V.; Choquet, P.; Saulot, A.; Filleter, T.; Colas, G. High Performance Space Lubrication of MoS2 with Tantalum. *Adv. Funct. Mater.* **2022**, *2110429*, 1–10. https://doi.org/10.1002/adfm.202110429.

(85) Ayerdi, J. J.; Aginagalde, A.; Llavori, I.; Bonse, J.; Spaltmann, D.; Zabala, A. Ball-on-Flat Linear Reciprocating Tests : Critical Assessment of Wear Volume Determination Methods and Suggested Improvements for ASTM D7755 Standard. *Wear* **2021**, *470–471* (January), 203620. https://doi.org/10.1016/j.wear.2021.203620.

(86) Pawel, P.; Rafal, R. Improvement of Wear Scar Volume Estimation in Reciprocating Motion. *Wear* **2025**, *572–573* (August 2024), 206023. https://doi.org/10.1016/j.wear.2025.206023.

(87) Lemesle, J.; Moreau, C.; Deltombe, R.; Blateyron, F.; Martin, J.; Bigerelle, M.; Brown, C. A. Top-down Determination of Fluctuations in Topographic Measurements. *Materials (Basel).* **2023**, *16*, 473.

(88) Moreau, C.; Lemesle, J.; Margarit, D. P.; Blateyron, F.; Bigerelle, M. A Statistical Approach for Characterizing the Behaviour of Roughness Parameters Measured by a Multi-Physics Instrument on Ground Surface Topographies : Four Novel Indicators. *Metrology* **2024**, *4*, 640–672.

(89) Schmitz, T. L.; Action, J. E.; Burris, D. L.; Ziegert, J. C.; Sawyer, W. G. Wear-Rate Uncertainty Analysis. *ASME J. Tribol.* **2004**, *126*, 802. https://doi.org/10.1115/1.1792675.

(90) Maculotti, G.; Goti, E.; Genta, G.; Mazza, L.; Galetto, M. Uncertainty-Based Comparison of Conventional and Surface Topography-Based Methods for Wear Volume Evaluation in Pin-on-Disc Tribological Test. *Tribol. Int.* **2022**, *165* (September 2021), 107260.

https://doi.org/10.1016/j.triboint.2021.107260.

(91) Qu, J.; Truhan, J. J. An Efficient Method for Accurately Determining Wear Volumes of Sliders with Non-Flat Wear Scars and Compound Curvatures ☪. *Wear* **2008**, *261* (2006), 848–855. https://doi.org/10.1016/j.wear.2006.01.009.

(92) Cornuault, P.-H.; Colas, G.; Lenain, A.; Daudin, R.; Gravier, S. On the Diversity of Accommodation Mechanisms in the Tribology of Bulk Metallic Glasses. *Tribol. Int.* **2020**, *141*, 105957. https://doi.org/10.1016/j.triboint.2019.105957.